A SHOCK-CAPTURING FINITE VOLUME SCHEME TO SOLVE 1D MULTI-LAYER SHALLOW WATER EQUATIONS

Silvia Bosa[1] & Marco Petti[1]

[1]Department of Chimica, Fisica e Ambiente, University of Udine, Italy, via Cotonificio 114, 33100 Udine

E-mail: silvia.bosa@uniud.it, marco.petti@uniud.it

Abstract

The multi-layer shallow water approach can be regarded as a development of De Saint Venant equations in the direction of a more accurate description of the physical problem, keeping as far as possible the efficiency of classical De Saint Venant numerical models. From this point of view, in the present paper, the one dimensional multi-layer De Saint Venant equations are briefly developed, marking the fact that the stresses due to the presence of neighboring layers can be treated as the effect of a virtual topography. In this way, continuity and momentum equation on each layer furnish a system of equations that is very similar to classic single-layer De Saint Venant equations.

This similitude suggests the possibility to solve the resulting differential equations by means of the techniques originally developed for the solution of De Saint Venant equations. Following this idea, the 1D multi-layer De Saint Venant equations are solved numerically by means of a shock-capturing finite volume technique applied to each layer separately.

The resulting numerical scheme is applied to some benchmark test, and the results are presented and discussed.

Introduction

The field of numerical modeling, finalized to hydraulic problems is very wide and it presents growing difficulties. The first difference among numerical models is due to the choice of the system of equations used to describe the physics of the natural phenomenon. Numerical models based on 3D Navier-Stokes equations are very heavy from a computational point of view and can be only applied to small computational domains, even if computers are always improving their performances. Due to this drawback, simpler versions of Navier-Stokes equations are still very useful, such as shallow water equations (SWE). To SWE belong dispersive equations (Boussinesq family) and non-dispersive equations (De Saint Venant family), that are easier to deal with.

The hydrostatic pressure distribution hypothesis seems to be not too strong in river hydraulics problems, so De Saint Venant equations have been widely applied in numerical schemes, particularly in combination with finite volume methods (FVM) for the numerical solution of the differential equations. The valuable results obtained, show that these schemes are a good compromise between accuracy and simplicity (e.g., Hervouet, 2000, Valiani et al., 2002, Begnudelli and Sanders, 2007, Liao et al., 2007, Shi and Nyugen, 2008, Gallegos et al., 2009, Bosa and Petti, 2011).

SWE are based on constant horizontal velocity distribution over the water depth. Thus, a further effort in the development of numerical models could be the introduction of a variable velocity distribution over the water depth. One way to deal in this direction is to consider a multi-layer distribution: the pressure distribution is still hydrostatic, but each layer is characterized by its own velocity, constant over the layer itself (e.g. Audusse, 2005, Bouchut and Zeitlin, 2010, Spinewine et al., 2011).

The paper is organized in the following manner. The governing equations are deduced in the following section and the adopted numerical scheme is presented. After that, the model is applied to some benchmark problems, divided between static tests and dam break tests. Finally, the results are discussed and compared with exact solution or with reference solution proposed in the literature.

Numerical model

Governing equations

With reference to a generic multi-layer problem, as depicted in Figure 1, the one-dimensional multi-layer shallow water equations can be derived applying the physical principles of mass and momentum conservation to

a control volume that include an infinitesimal stretch of generic layer *l*.

In this paper, the equations are developed for inviscid flow, thus all flow resistances are neglected. Moreover the fluid is considered to be the incompressible and the layers are non-miscible. The usual approximation is adopted of mild bottom slope and gradually varying layer water depth. Under these assumptions, continuity equation for layer *l* is:

$$\frac{\partial h_l}{\partial t}+\frac{\partial U_l h_l}{\partial x}=0 \tag{1}$$

being (*t*, *x*) temporal and horizontal spatial coordinate, h_l water depth of layer *l* and U_l mean flow velocity of layer *l* in *x*- direction.

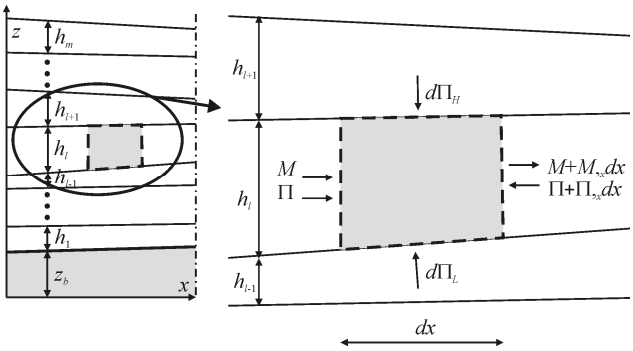

Figure 1. Subdivision of water depth in *m* layers and a detail of momentum equation on a generic control volume.

Momentum equation along *x*- direction can be written on the considered control volume (Figure 1) as:

$$dI+\frac{\partial M}{\partial x}dx=-\frac{\partial \Pi}{\partial x}dx-d\Pi_L\frac{\partial\left(z_b+\sum_{j=1}^{l-1}h_j\right)}{\partial x}+ +d\Pi_H\frac{\partial\left(z_b+\sum_{j=1}^{l}h_j\right)}{\partial x} \tag{2}$$

being *dI*, *M*, and Π the component in *x* direction of the local inertia, the momentum and the hydrostatic force on the face orthogonal to *x* axis; $d\Pi_L$ and $d\Pi_H$ are the hydrostatic forces acting on the lower and higher faces of the control volume; z_b is the bottom height.

The forces Π, $d\Pi_L$ and $d\Pi_H$ are evaluated by means of the hydrostatic pressure; thus, with some algebraic manipulation (Bouchut and Zeitlin, 2010), momentum equation becomes:

$$\frac{\partial U_l h_l}{\partial t}+\frac{\partial\left(U_l{}^2 h_l+g h_l{}^2/2\right)}{\partial x}= =-g h_l\frac{\partial}{\partial x}\left(z_b+\sum_{j=1}^{l-1}h_j+\sum_{j=l+1}^{m}\frac{\rho_j}{\rho_l}h_j\right) \tag{3}$$

being *g* the gravity acceleration and ρ_j the density of layer *j* and *m* the total number of layers.

Finally the system of equations that describes the motion of the fluid is:

$$\begin{cases}\dfrac{\partial h_l}{\partial t}+\dfrac{\partial U_l h_l}{\partial x}=0\\ \dfrac{\partial U_l h_l}{\partial t}+\dfrac{\partial\left(U_l{}^2 h_l+g h_l{}^2/2\right)}{\partial x}= \\ =-g h_l\dfrac{\partial}{\partial x}\left(z_b+\sum_{j=1}^{l-1}h_j+\sum_{j=l+1}^{M}\dfrac{\rho_j}{\rho_l}h_j\right)\end{cases} \qquad l=1,\ldots,m \tag{4}$$

The structure of equation (4) is very similar to the one of a single layer system:

$$\begin{cases}\dfrac{\partial h}{\partial t}+\dfrac{\partial U h}{\partial x}=0\\ \dfrac{\partial U h}{\partial t}+\dfrac{\partial\left(U^2 h+g h^2/2\right)}{\partial x}=-g h\dfrac{\partial z_b}{\partial x}\end{cases} \tag{5}$$

with *h* water depth and *U* mean velocity of the flow in *x*-direction. This fact suggests to introduce a new variable associated to layer *l*, z_{vl}, that acts as a virtual topography (Bouchut and Zeitlin, 2010):

$$z_{vl}=z_b+\sum_{j=1}^{l-1}h_j+\sum_{j=l+1}^{m}\frac{\rho_j}{\rho_l}h_j \ . \tag{6}$$

As underlined in equation (6) the virtual topography depends on the layer *l*, and on (*x*, *t*) coordinates. It takes into account the bottom height and the pressure-driven terms arising from $d\Pi_L$ and $d\Pi_H$. Hence, with the introduction of z_{vl}, equation (4) becomes:

$$\begin{cases}\dfrac{\partial h_l}{\partial t}+\dfrac{\partial U_l h_l}{\partial x}=0\\ \dfrac{\partial U_l h_l}{\partial t}+\dfrac{\partial\left(U_l{}^2 h_l+g h_l{}^2/2\right)}{\partial x}=-g h_l\dfrac{\partial z_{vl}}{\partial x}\end{cases} \qquad l=1,\ldots,m \tag{7}$$

Using the chain rule, it is possible to derive other versions of multi-layer SWE, with different level of coupling of the pressure-driven terms (Spinewine et al., 2011). Equation (7) is characterized by a complete decoupling, with all pressure-driven terms on the right hand side of the equation.

This form is particularly attractive, because each layer can be solved separately, following the same strategies used in the numerical integration of equation (5) and presented in a wide literature (e.g. Alcrudo et al., 1993, Toro, 2001, Zhou et al., 2001, Liang and Borthwick, 2009).

Numerical scheme

Equation (7) is here expressed in a matrix form for a two – layer scheme:

$$\frac{\partial}{\partial t}\begin{pmatrix}\mathbf{U}_1\\ \mathbf{U}_2\end{pmatrix}+\frac{\partial}{\partial x}\begin{pmatrix}\mathbf{F}_1\\ \mathbf{F}_2\end{pmatrix}=\begin{pmatrix}\mathbf{S}_1\\ \mathbf{S}_2\end{pmatrix} \tag{8}$$

with

$$\mathbf{U}_l=\begin{pmatrix}h_l\\ U_l h_l\end{pmatrix};\mathbf{F}_l=\begin{pmatrix}U_l h_l\\ U_l{}^2 h_l+\dfrac{g h_l{}^2}{2}\end{pmatrix};\qquad l=1,2$$

$$\mathbf{S}_1=\begin{pmatrix}0\\ -g h_1\dfrac{\partial z_{v1}}{\partial x}\end{pmatrix}=\begin{pmatrix}0\\ -g h_1\dfrac{\partial\left(z_b+\chi h_2\right)}{\partial x}\end{pmatrix}; \tag{9}$$

$$\mathbf{S}_2=\begin{pmatrix}0\\ -g h_2\dfrac{\partial z_{v2}}{\partial x}\end{pmatrix}=\begin{pmatrix}0\\ -g h_2\dfrac{\partial\left(z_b+h_1\right)}{\partial x}\end{pmatrix};$$

being $\chi = \rho_2/\rho_1$.

The numerical integration is carried out by means of a scheme that solves equation (8) for each layer at each time step. In this way the pressure-driven term that represents the influence of layer 2 on layer 1 (and vice versa) is computed in the virtual topography z_{v1} (z_{v2}), that is evaluated at the previous time step.

The spatial integration domain is discretized in a number of cells, being $\Delta x_i = x_{i+1/2} - x_{i-1/2}$ the length of generic cell i. In this context, the discretized variable is referred to the cell centre, so as an example $h_{l,i}{}^n$ is the water depth of layer l in cell i at the time step t^n.

The time marching formula adopted is first order accurate and it can be written in compact form as:

$$\mathbf{U}_{l,i}{}^{n+1}=\mathbf{U}_{l,i}{}^{n}+\frac{\Delta t}{\Delta x_i}\left[\mathbf{F}_{l,i-1/2}^{HLL,R}+\mathbf{F}_{l,i+1/2}^{HLL,L}\right]. \tag{10}$$

The advective fluxes in equation (10) are calculated applying the LHLL Riemann solver (Fraccarollo et al., 2003), that introduces the effect of the bottom slope as a correction of the numerical flux, instead of treating it as a source term. Here the scheme is extended to incorporate the effect of the whole virtual topography in the fluxes.

The idea behind this solver can be easily explained writing the momentum equation for layer l on a control volume that includes the discontinuity at i+1/2 (Figure 2). In discretized form, the surface elevation and virtual topography are actually constant throughout each cell. It can be shown that the difference between the dynamic forces acting on the left and right hand side of the discontinuity must be equal to the thrust term on the step, named D and assumed as:

$$\mathbf{F}_{l,i+1/2}^{HLL,L}-\mathbf{F}_{l,i+1/2}^{HLL,R}=D=$$

$$=g\frac{h_{l,i}{}^n+h_{l,i+1}{}^n}{2}\left(z_{vl,i+1}{}^n-z_{vl,i}{}^n\right). \tag{11}$$

Following Fraccarollo et al. (2003) this can be reached first applying a classical HLL solver (Harten et al., 1983):

$$\mathbf{F}_{l,i+1/2}^{HLL}=\frac{S_R\mathbf{F}_L-S_L\mathbf{F}_R+S_L S_R\left(\mathbf{U}_R-\mathbf{U}_L\right)}{S_R-S_L} \tag{12}$$

with

$$\mathbf{U}_L=\mathbf{U}_{l,i}{}^n;\mathbf{U}_R=\mathbf{U}_{l,i+1}{}^n; \tag{13}$$

$$\mathbf{F}_L=\begin{pmatrix}U_{l,i}{}^n h_{l,i}{}^n\\ \left(U_{l,i}{}^n\right)^2 h_{l,i}{}^n+g\left(h_{l,i}{}^n\right)^2/2\end{pmatrix};$$

$$\mathbf{F}_R=\begin{pmatrix}U_{l,i+1}{}^n h_{l,i+1}{}^n\\ \left(U_{l,i+1}{}^n\right)^2 h_{l,i+1}{}^n+g\left(h_{l,i+1}{}^n\right)^2/2\end{pmatrix} \tag{14}$$

and then computing a correction:

$$\mathbf{F}_{l,i+1/2}^{HLL,K}=\mathbf{F}_{l,i+1/2}^{HLL}-\frac{S_K}{S_R-S_L}g\frac{h_{l,i}{}^n+h_{l,i+1}{}^n}{2}\cdot$$

$$\cdot\begin{pmatrix}0\\ z_{vl,i+1}{}^n-z_{vl,i}{}^n\end{pmatrix}\qquad K=L,R. \tag{15}$$

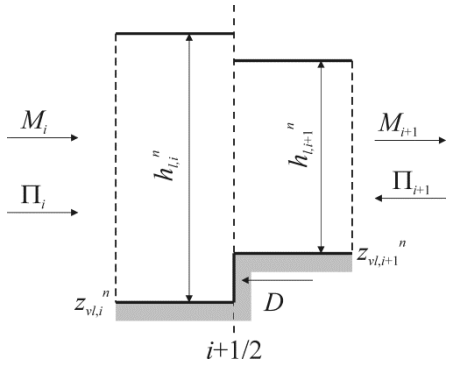

Figure 2. Idea behind LHLL solver: momentum equation on a control volume across the discontinuity.

In this way the first component of the flux evaluated through LHLL and HLL does not change, as expected, being the continuity equation conservative. On the other hand side the jump of the second component of the flux across the intercell i+1/2 is consistent with equation (11).

In the original formulation of HLL, S_L and S_R are the wave speed of the left and right wave in the solution of the local Riemann problem and can be evaluated using several approaches (Toro, 2001). One have to keep in mind that the original formulation gives rise to only two waves.

To keep the bottom height on the left hand side instead of in the source term, Fraccarollo et al. (2003) analyze a generalized eigenvalue problem that gives origin to three waves. So, they consider the eigenvalues associated to the leftmost wave evaluated on cell i and i+1 and the minimum is chosen to be S_L; on the other hand side S_R is the maximum eigenvalue associated to the rightmost wave evaluated on cell i and i+1.

In the same way, in the present formulation, to keep the virtual topography term on the left hand side instead of in the source term, the characteristic wave speeds should be evaluated seeking the eigenvalues on the Jacobian matrix of

the full coupled equation system. Unfortunately, exact eigenvalues of this matrix in the general case cannot be found using simple algebraic expression; moreover, they may become complex under certain conditions. Nevertheless, Spinewine et al. (2011) provide a lower and upper bounds of their modulus:

$$\begin{cases} \lambda^n_{\min,i} = \min\left(U^n_{1,i}, U^n_{2,i}\right) - \sqrt{g\left(h^n_{1,i} + h^n_{2,i}\right)} \\ \lambda^n_{\max,i} = \max\left(U^n_{1,i}, U^n_{2,i}\right) + \sqrt{g\left(h^n_{1,i} + h^n_{2,i}\right)} \end{cases} \quad (16)$$

Thus, following values are adopted:

$$\begin{cases} S_L = \min\left\{0, \lambda^n_{\min,i}, \lambda^n_{\min,i+1}\right\} \\ S_R = \max\left\{0, \lambda^n_{\max,i}, \lambda^n_{\max,i+1}\right\} \end{cases}. \quad (17)$$

To ensure the *C*-property to be satisfied, when the local velocities approach zero value, the water level ($\eta_l = z_{vl}+h_l$) is used instead of water depth (h_l) as the first component of U_l in (9).

Moreover, the method proposed by Liang and Borthwick (2009) is used to modify flow variables so as not to induce spurious flow in dry areas.

The resulting numerical scheme is first order accurate both in space and time. As the adopted scheme is explicit, the usual Courant condition must hold, i.e.

$$\Delta t = Cr \frac{\Delta x_{\min}}{S_{\max}} \quad (18)$$

with $\Delta x_{\min}$ the minimum cell size over the mesh, $S_{\max}$ the maximum characteristic wave speed estimated as:

$$S_{\max} = \max_{l,i}\left(U_{l,i}{}^n\right) + \sqrt{g \max_i\left(h_{1,i}{}^n + h_{2,i}{}^n\right)}. \quad (19)$$

For the Courant number *Cr*, value *Cr* = 0.5 is adopted in all the computations reported hereafter.

Numerical applications

The numerical scheme is validated against some benchmark tests originally proposed by Spinewine et al. (2011) and Bouchut and Zeitlin (2010).

Static tests

The first test (ST1) consists of two layers having the same density at rest in a 1000 m long horizontal channel. The initial conditions are characterized by a free surface located 10 m over the bottom height and a discontinuity in the layers depth at x = 500 m. In this test the exact solution is the same as the initial condition, due to the constancy of fluid density. The cell size is Δx = 1 m; the results after 500 s are shown in Figure 3.

In the second static test (ST2) two layers of the same density are at rest over a 1000 m long piecewise horizontal channel, with a bottom discontinuity at x = 500 m. Initially, the free surface and the interface between the layers are horizontal. The cell size is Δx = 1 m; the results after 500 s are shown in Figure 4. Also in this test the exact solution is the same as the initial condition, nevertheless, unlike ST1, here the numerical results manifest a spurious oscillation at the discontinuity.

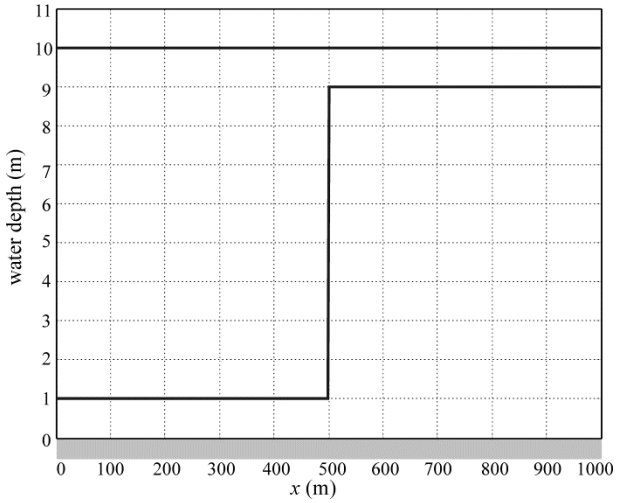

Figure 3. Numerical solution of ST1 after 500s.

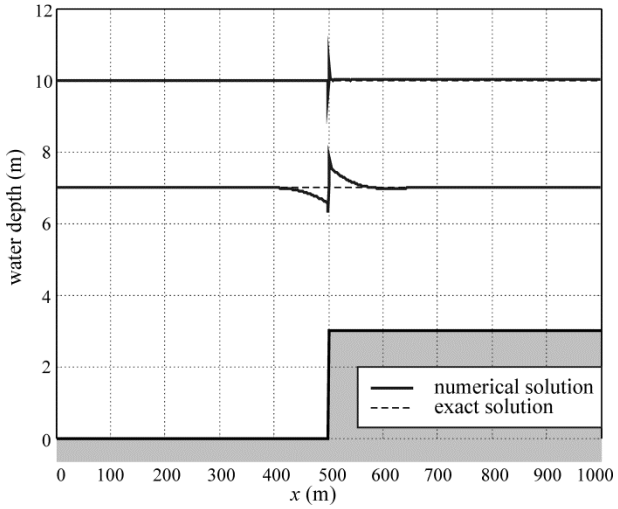

Figure 4. Numerical and exact solution of ST2 after 500s.

Dam break tests

In the following, six dam break tests are presented (DB1 to DB6). All of them are characterized by a horizontal bed with height z_b and length L; the initial discontinuity is located at $x = x_0$. The initial depth of the layers is h_{1L} and h_{2L} on the left hand side of the channel and h_{1R} and h_{2R} on the right hand side. The initial velocities are equal in both layers and are zero everywhere with the only exception of test DB5. The ratio of the fluid densities is χ. The grid size is Δx and the duration of the simulations is $t_{\max}$. The data used in all dam break tests are summarized in Tables 1 and 2 and in Figure 5.

The results of DB1 and DB2 (Figures 6 and 7) show a very good agreement with exact solution in the free surface, while the sharp discontinuity at the interface between layer 1 and 2 is slightly smoothed in both tests. This could be

ascribed to the fact that the numerical scheme adopted is still first order accurate in space.

Table 1. Setup data of dam break tests.

test	z_b (m)	L (m)	x_0 (m)	χ (-)	t_{max} (s)	Δx (m)
DB1	0.000	1000	500	1	25	0.1
DB2	-0.357	10000	5000	1	800	1
DB3	-0.357	10000	5000	0.05	800	1
DB4	-0.357	10000	5000	0.2	800	1
DB5	0.000	1	0.5	0.98	0.05	0.01
DB6	0.000	10	5	0.7	1	0.02

Table 2. Initial conditions of dam break tests.

test	h_{1L} (m)	h_{1R} (m)	h_{2L} (m)	h_{2R} (m)	$U_{1L} = U_{1R} = U_{2L} = U_{2R}$ (m/s)
DB1	0	1	10	0	0.0
DB2, DB3, DB4	0.357	0.357	1	0	0.0
DB5	0.5	0.45	0.5	0.55	2.5
DB6	0.2	1.8	1.8	0.2	0.0

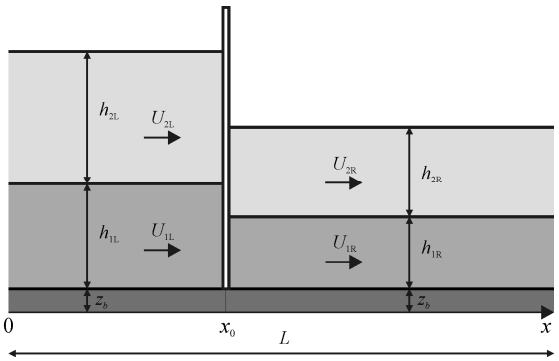

Figure 5. Symbols used to describe the initial conditions of dam break tests.

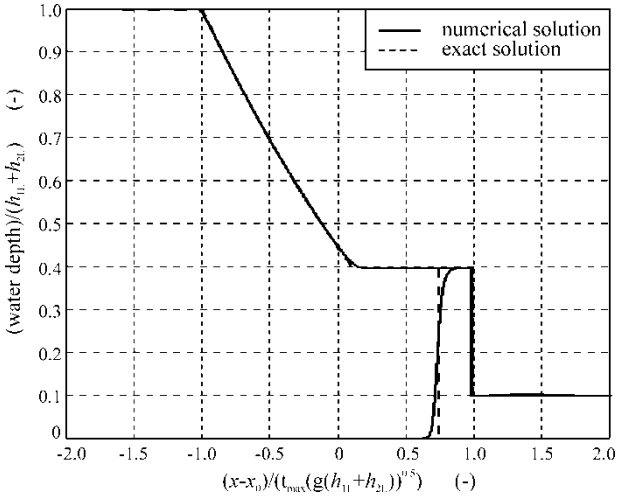

Figure 6. Numerical and exact solution of DB1.

DB3 does not have an exact solution, thus as a reference solution the exact solution for $\chi = 0$ has been chosen (Figure 8). From a engineering point of view, this means that $\rho_1 \gg \rho_2$, i.e. layer 1 can be considered at rest and layer 2 moves on it, thus this represents a dam break of layer 2 over a fixed bed made by $z_b + h_1$. The numerical result obtained with $\chi = 0.05$ approaches the reference solution, with a deviation probably due to the fact that $\chi \neq 0$.

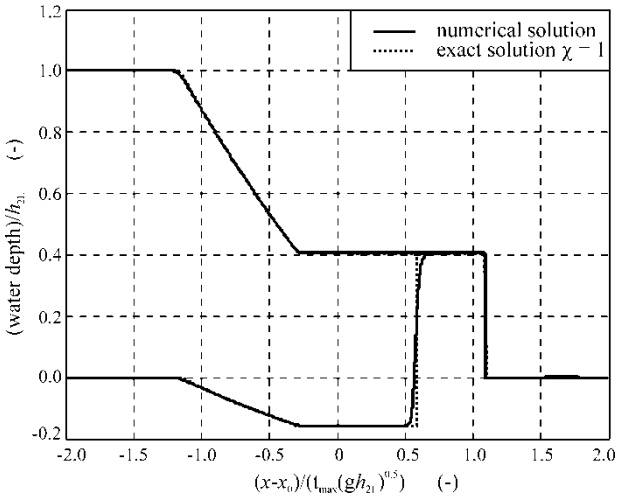

Figure 7. Numerical and exact solution of DB2.

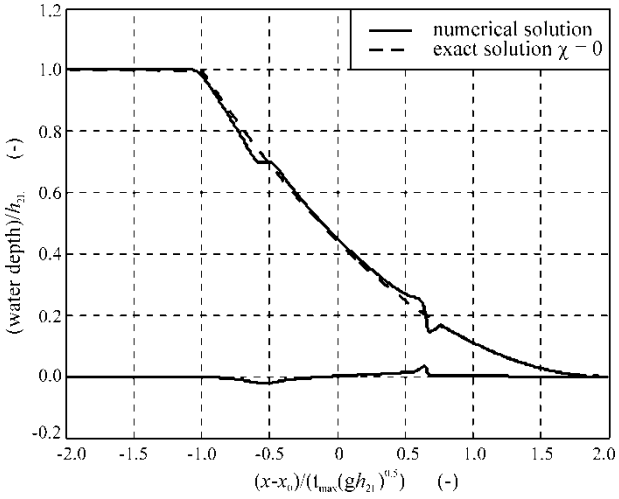

Figure 8. Numerical and reference solution of DB3.

Test DB4 represent a middle ground between test DB2 and test DB3, with $\chi = 0.2$. Thus, in Figure 9 the numerical results are depicted together with both reference solutions ($\chi = 1$ and $\chi = 0$). As expected, numerical results fall in between the results of DB2 and DB3, according with Spinewine et al. (2011).

The results of tests DB5 and DB6 are depicted in Figures 10 and 11 as the interfaces between layer 1 and 2, together with the reference solutions proposed by Bouchut and Zeitlin (2010). Again the sharp discontinuity of the reference solution is smoothed by the first order numerical scheme, nevertheless, the trend of the solution in its substance is well represented, with no sensible spurious oscillations.

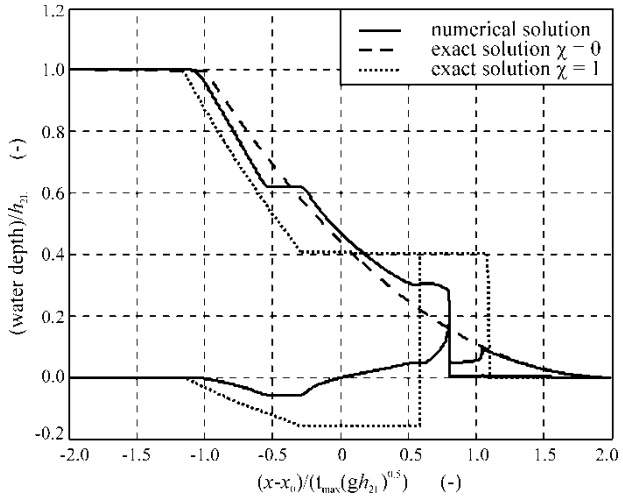

Figure 9. Numerical and reference solutions of DB4.

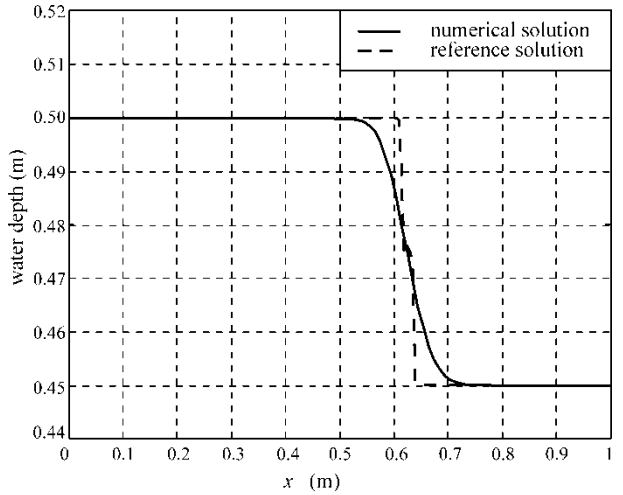

Figure 10. Numerical and exact solution of DB5.

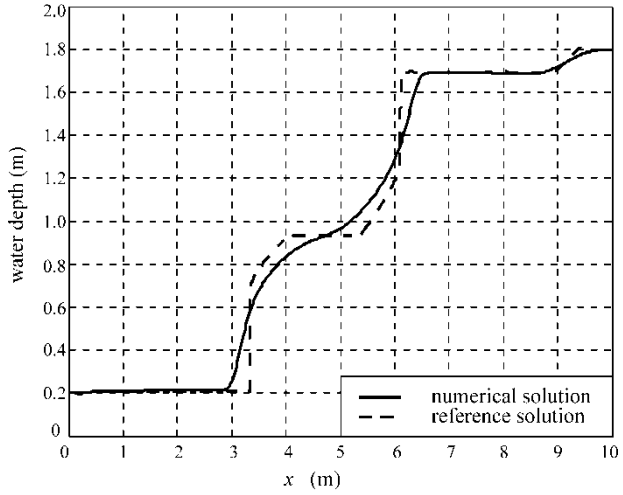

Figure 11. Numerical and exact solution of DB6.

Conclusions

In the present paper the multi-layer De Saint Venant equations were developed. Their particular structure is very similar to single-layer De Saint Venant equations, with a virtual topography to account not only for the bottom height, but also for the pressure due to the above and below layers.

This suggested the possibility to approach the numerical integration of multi-layer De Saint Venant equations with techniques, similar to those applied to single layer problems, that have been widely tested in the reference literature. In this way a numerical scheme was developed for the two-layer case, with particular care to the treatment of the source term due to the virtual topography.

The derived numerical model was applied to some benchmark tests and the results show a good representation of physical problems, with some difficulties reproducing sharp discontinuities, probably due to the fact that the scheme is still first order accurate.

Thus, further developments can be addressed to the implementation of second order accuracy both in space and time.

References

Alcrudo, F., Garcìa-Navarro, P. (1993). A high-resolution Godunov-type scheme in finite volumes for the 2D shallow-water equations. *Int J Numer Fluids*, 16, 489-505.

Audusse, E. (2005). A multilayer Saint-Venant model: derivation and numerical validation. *Discrete Conti Dyn-B* 5(2), 189-214.

Begnudelli, L., & Sanders B.F. (2007). Simulation of the St.Francis dam-break flood. *Journal of Engineering Mechanics*, 133, 1200-1212.

Bosa, S., & Petti, M. (2011). Shallow water numerical model of the wave generated by the Vajont landslide. *Environmental Modelling & Software*, 26, 406-418, DOI: 10.1016/j.envsoft.2010.10.001.

Bouchut, F., & Zeitlin, V. (2010). A robust well-balanced scheme for multi-layer shallow water equations. *Discrete Conti Dyn-B* 13, 739-758.

Fraccarollo, L., Capart, H., & Zech Y. (2003). A Godunov method for the computation of erosional shallow water transients. *Int J Numer Meth Fl*, 41, 951-976.

Gallegos, H.A., Schubert, J.E., & Sanders, B.F. (2009). Two-dimensional, high-resolution modeling of urban dam-break flooding: a case study of Baldwin Hills, California. *Advances in Water Resources*, 32, 1323-1335.

Harten, A., Lax, P.D., & van Leer, B. (1983). On upstream differencing and Godunov-type schemes for hyperbolic conservation laws. *SIAM Rev*, 25 (1), 35-61.

Hervouet, J.-M. (2000). A high resolution 2-D dam-break model using parallelization. *Hydrol Process*, 14, 2211-2230.

Liang, Q., & Borthwick, A.G.L. (2009). Adaptive quadtree simulation of shallow flows with wet-dry fronts over complex topography. *Comput Fluids*, 38, 221-234.

Liao, C.B., Wu, M.S., Liang, S.J. (2007). Numerical simulation of a dam break for an actual river terrain environment. *Hydrol Process*, 21, 447-460.

Shi, Y., & Nyugen, K.D. (2008). A projection method-based model for dam- and dyke-break flows using an unstructured finite-volume technique: Applications to the Malpasset dam break (France) and to the flood diversion in the Red River Basin (Vietnam). *Int. J. Numer. Meth. Fluids*, 56, 1505-1512.

Spinewine, B., Guinot, V., Soares-Frazão, S., & Zech, Y. (2011). Solution properties and approximate Riemann solvers for two-layer shallow flow models. *Comput Fluids*, 44, 202-220.

Toro, E.F. (2001). *Shock-capturing methods for free-surface shallow flows*. John Wiley and Sons, LTD.

Valiani, A., Caleffi, V., & Zanni, A. (2002). Case study: Malpasset dam-break simulation using a two-dimensional finite volume method. *Journal of Hydraulic Engineering*, 128, 460-472.

Zhou, J.G., Causon, D.M., Mingham, C.G., Ingram, D.M. (2001). The Surface Gradient Method for the treatment of source terms in the shallow-water equations. *J Comput Phys*, 168, 1-25.